ACS APPLIED NANO MATERIALS

www.acsanm.org Article

Virtual Screening of Nanoporous Materials for Noble Gas Separation

Jingqi Wang, Musen Zhou, Diannan Lu,* Weiyang Fei, and Jianzhong Wu*

Cite This: https://doi.org/10.1021/acsanm.1c03907 Read Online

ACCESS | Metrics & More | Article Recommendations | Supporting Information

ABSTRACT: Noble gases are vital industrial chemicals widely used in various applications, such as cryogenics and optical devices. Compared with conventional technologies for the enrichment and separation of noble gases from the atmosphere, emerging methods based on advanced nanoporous materials have advantages in terms of energy and separation efficiency due to their tunable pore structure and chemical affinities. In this work, both sorption and transport properties are calculated via efficient theoretical models to screen large experimental libraries of nanoporous materials to enrich argon, krypton, and xenon from various mixtures. The theoretical predictions are validated by Monte Carlo simulation and molecular dynamics simulation. Promising candidates are identified for both adsorption separation and membrane separation of Ar/Kr, Kr/Xe, and Xe/Ar. The structure−property relation identified in this work provides insights for the design of nanoporous materials in noble gas separation.

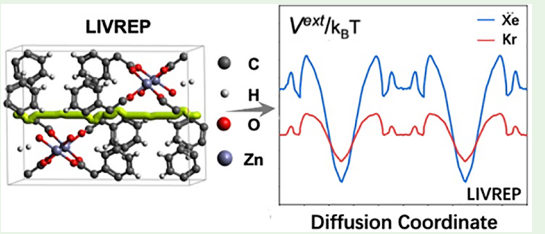

KEYWORDS: *high-throughput screening, theory, noble gas separation, metal−organic framework (MOF), adsorption, diffusion coefficient, Monte Carlo (MC), molecular dynamics (MD) simulation*

1. INTRODUCTION

Noble gases are valuable commodities in the chemical industry. Among the six naturally occurring noble gases, helium (He), neon (Ne), argon (Ar), krypton (Kr), xenon (Xe), and radon (Ra), argon has been widely used for thermal insulation and commercial lighting; krypton is commonly used in leak testing and excimer lasers; and xenon has broad applications in neutron counters and medical fields such as neuroprotection and anesthetics.[1,2] For most industrial uses, the noble gases are enriched from the Earth's atmosphere, which contains about 0.94% of noble gases by volume. While argon accounts for the overwhelming majority of noble gases in the atmosphere, with a concentration of 9340 ppm under the ambient condition, the concentration of xenon is 0.087 ppm, and that for krypton is 1.14 ppm.[3,4] Because of low concentration yet a high commercial value, krypton and xenon have extremely high market prices about 120.3 and 767.8 USD/kg, respectively, while argon, only 3.1 USD/kg, is much cheaper due to its abundance.[5]

The industrial separation of noble gases often starts with a byproduct from the cryogenic distillation of the atmosphere with a 4:1 molar ratio of krypton and xenon.[6,7] Accordingly, the gas mixture is often used as a model system for the industrial design and optimization of noble gas enrichment and separation processes. To generate pure gas products, the noble gas mixture typically goes through further cryogenic distillation with the separation efficiency depending only on the difference in volatility. As a result, the conventional process for the separation of noble gases is energy- and cost-intensive.[8] Alternatively, more energy-efficient processes, such as adsorption and membrane separation, are desirable to satisfy industrial needs. Toward that end, the use of nanoporous materials such as metal−organic frameworks (MOFs) and covalent−organic frameworks (COFs) are very promising.[9] Figure 1 shows the structure and chemical composition of MOF and COF materials. MOFs are a class of crystalline materials consisting of metallic clusters and organic linkers, where metallic clusters are linked to organic linkers with coordination bonds.[10,11] In comparison to MOFs, COFs are

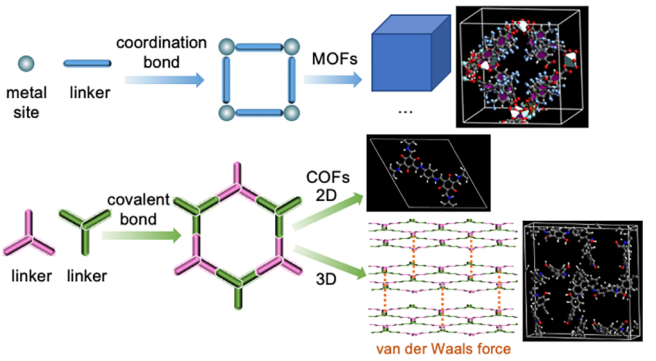

Figure 1. Illustration of structure and chemical composition in MOF/COF materials.

Received: December 16, 2021
Accepted: January 25, 2022

https://doi.org/10.1021/acsanm.1c03907
ACS Appl. Nano Mater. XXXX, XXX, XXX−XXX

also crystalline porous materials but composed of lighter elements (e.g., H, C, N, and O) where different organic linkers are connected by covalent bonds, which makes COFs more lightweight than MOFs.[12,13] Different from MOFs, two-dimensional layered structures exist in COFs where interlayer interaction is governed by van der Waals force. The modular nature in both MOFs and COFs enables the design and synthesis of large groups of candidates with tunable aperture sizes, large specific surface areas, and periodic characteristics.[14,15] The structural features and local chemical composition make MOFs and COFs excellent candidates for gas adsorption and separation.

Recent years, nanoporous materials such as MOFs and COFs have been studied to improve the separation performance of noble gases by both experimental and computational methods.[16−18] Although experimental synthesis has led to the discovery of many novel MOFs and COFs promising for water harvesting[19] and gas storage and separation,[20−23] the extensive labor and time cost of experimental synthesis of nanoporous materials make it impossible to explore the almost infinite structure configuration space of nanoporous materials, whereas computational methods are able to provide fast yet accurate prediction of materials' properties before experimental synthesis. For noble gas separation, most literature studies using computational methods are only focused on the adsorption separation.[17,24−27] In principle, membrane separation would be more efficient than adsorption separation because it leverages both sorption and transport properties to separate gas molecules. However, the systematic evaluation of transport properties (e.g., self-diffusion coefficient) for noble gas molecules in nanoporous materials is still absent because it is computationally prohibitive for conventional molecular simulation methods (viz., molecular dynamics) to predict the self-diffusion coefficient for a large structure database of nanoporous materials.

In this work, we investigate the potential use of MOFs and COFs as both adsorbents or membranes to enrich and separate noble gases. By considering both sorption and transport properties (viz., Henry's constant and diffusion coefficient) via efficient theoretical methods for argon, krypton, and xenon in a large nanoporous material database, we identified the top candidates for the adsorption separation and membrane separation of binary noble gas mixtures. The separation selectivity and capacity predicted by theoretical methods are further verified by Monte Carlo and molecular dynamics (MD) simulation for top MOF and COF candidates. The material database consists of 10,143 computation-ready, experimental MOFs (CoRE MOF 2019)[28,29] and 449 computation-ready, experimental COFs (CoRE COF 2019).[12,30] Similar to other high-throughput screening work,[25,26,31,32] all the MOFs and COFs are treated as rigid for fast screening for the noble gas separation. Although the flexibility of nanoporous materials might affect the separation performance,[33] the computational modeling of flexibility is heavily relied on the force field and exact impact of flexibility for top nanoporous materials identified in noble gas separation shall be carefully investigated experimentally before further scale-up. The comparison between virtually all MOF and COF materials synthesized so far reveals that their performances for the enrichment and separation of noble gases are related to the framework structure and composition. The structure−performance relationships can further guide materials design and process optimization.

2. METHODS

2.1. Molecular Model. In this work, intermolecular interactions are represented by the standard Lennard-Jones (LJ) model. Table 1 provides the LJ size and energy parameters of noble gas molecules (i.e., argon, krypton and xenon) estimated from the principle of corresponding states for the second virial coefficients.[9,34] The Lorentz−Berthelot mixing rule is used to describe the LJ parameters for the interactions between different species. The LJ parameters of atoms in MOFs or COFs are described by the universal force field (UFF), which is a standard force field to evaluate molecular adsorption and diffusion in nanoporous materials.[35] A cutoff of 12.9 Å is used for the calculation of all interatomic energies.

Table 1. LJ Size and Energy Parameters for Argon, Krypton, and Xenon

	σ (Å)	ε/k_B (K)
Ar	3.41	119.5
Kr	3.66	165.2
Xe	3.97	229.8

2.2. Adsorption Selectivity. We apply the ideal adsorption solution theory (IAST)[36] to evaluate the performance of different nanoporous materials (MOFs and COFs) for the separation of noble gases by adsorption processes. At a given temperature, the ideal adsorption selectivity is defined by the ratio of Henry's constants[36]

$$\alpha^{\mathrm{IM}} = K_{\mathrm{h},2}/K_{\mathrm{h},1} \tag{1}$$

where the superscript IM represents an ideal mixture; i.e., there is no interaction between gas molecules in bulk or at the adsorbed state. Henry's constant is determined from the external potential $V^{\mathrm{ext}}(\boldsymbol{r})$ for the gas molecule[37]

$$K_{\mathrm{h}} = \frac{1}{\Omega}\int \mathrm{d}\boldsymbol{r}\exp\left[-\frac{V^{\mathrm{ext}}(\boldsymbol{r})}{k_{\mathrm{B}}T}\right] \tag{2}$$

where Ω represents the system volume, T is the absolute temperature, and k_B is the Boltzmann constant. The detailed derivations of Henry's constant are also provided in the Supporting Information. For an ideal gas, the adsorption amount per unit volume is proportional to pressure and Henry's constant.

2.3. Membrane Selectivity. Nanoporous material can be used either as an adsorbent or as a selective membrane for gas separation. In Henry's law region (viz., at low pressure), the membrane selectivity is related to the ratio of Henry's constants multiplied by the ratio of the diffusivity coefficients at infinite dilution:[37,38]

$$k^{\mathrm{IM}} = \frac{K_{\mathrm{h},2}}{K_{\mathrm{h},1}}\frac{D_{0,2}}{D_{0,1}} = \frac{P_2}{P_1} \tag{3}$$

In eq 3, permeability P is defined as the product of Henry's constant, K_h, and self-diffusion coefficient D_0 at infinite dilution.[37] The latter can be predicted from the transition-state theory (TST).[37,39] For noble gas in a porous material, the diffusion coefficient can be estimated via molecular hopping between neighboring cages:

$$D_0 = \frac{1}{2}\varpi a^2 \tag{4}$$

where a stands for the distance between the initial and final states of molecular hopping (i.e., unit cell length along the direction of diffusion), and ϖ represents the hopping rate or the transmission frequency. According to TST, ϖ can be calculated from[40]

$$\varpi = \sqrt{\frac{k_{\mathrm{B}}T}{2\pi m}}\frac{\exp[-V^{\mathrm{ext}}(s^*)/k_{\mathrm{B}}T]}{\int_0^1 \exp[-V^{\mathrm{ext}}(s)/k_{\mathrm{B}}T]\mathrm{d}s} \tag{5}$$

where m stands for the molecular mass, s is defined as a normalized diffusion coordinate ($0 \le s \le 1$) that connects the initial ($s = 0$) and

https://doi.org/10.1021/acsanm.1c03907
ACS Appl. Nano Mater. XXXX, XXX, XXX−XXX

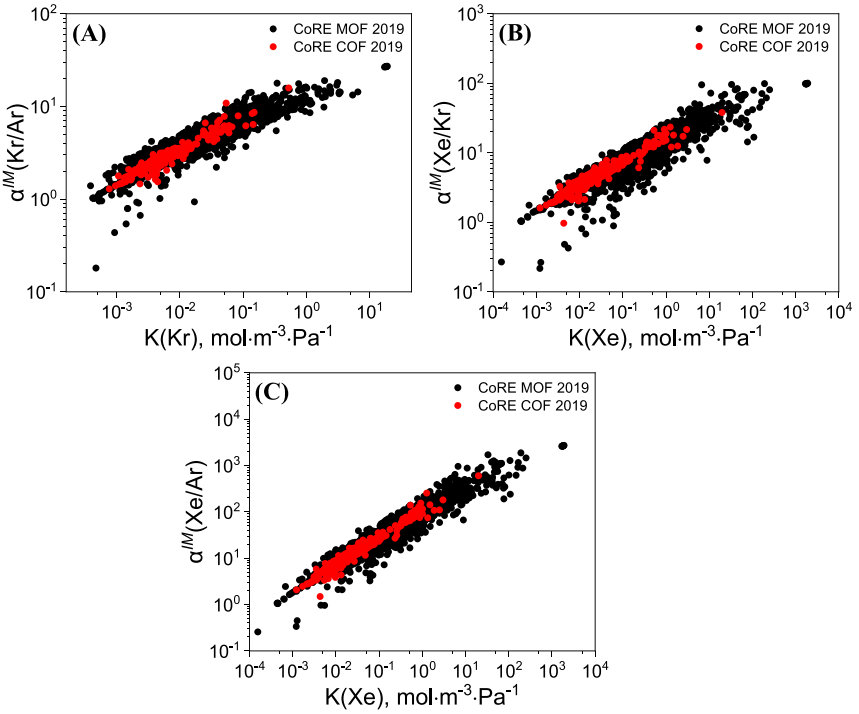

Figure 2. Ideal adsorption selectivity versus Henry's constant for both MOFs and COFs from the CoRE 2019 database for the separation of (A) Kr/Ar, (B) Xe/Kr, and (C) Xe/Ar at 300 K.

final (s = 1) states of gas hopping, and the integral is carried over the diffusion coordinate. The superscript * denotes the transition state for gas hopping between neighboring cages. The numerical details of the string method for minimum energy path (MEP) of gas molecules in nanoporous materials can be found in our previous work.[41] Despite the simplicity of TST, once accurate MEP is obtained, the predicted self-diffusion coefficients are in excellent agreement with those calculated from MD simulations.[41−43] More importantly, it would be computationally prohibitive to use MD simulations for large-scale screening of self-diffusion coefficients, especially for slow diffusion. To study the effects of the material structure on the separation efficiency, we use Zeo^{++}[44] software (with UFF) to analyze the structural features of the promising candidates. These structural features include the largest cavity diameter (LCD), pore limiting diameter (PLD), void fraction, void volume, and specific surface area.

2.4. Molecular Simulation. In this work, molecular simulations, including grand canonical Monte Carlo (GCMC) simulation and MD simulation, are used to verify sorption and transport properties calculated from the theoretical models. For sorption properties, GCMC simulation is carried out with RASPA, 5×10^6 steps were performed as the initialization cycles, and another 5×10^6 steps were performed to sample the adsorption capacity.[45,46] For transport properties, MD simulation is used to evaluate the diffusion coefficient of the optimal MOF and COF membrane via LAMMPS.[47] In MD simulation, 1 ns was used for equilibration and another 10 ns is used for production. The diffusion coefficient in MD simulation is calculated from mean-square displacement via the Einstein equation.

$$D_0 = \frac{1}{n}\lim_{t\to\infty}\frac{|\vec{r}(t) - \vec{r}(0)|^2}{2t} \tag{6}$$

where n is the number of dimensions, t represents the time, and r stands for the coordinate of the gas molecules. Three simulations intervals are used to obtain the average and the standard deviation. For both GCMC and MD simulations, the system temperature, cutoff, and force field parameters are the same as those in our theoretical calculations. All the unit cell in the simulation box is duplicated so that each axis is at least two times the cutoff.

3. RESULTS AND DISCUSSION

3.1. Selectivity of MOFs and COFs as Adsorbents. In this work, we explore the applicability of MOFs and COFs either as adsorbents or as selective membranes for the separation of binary noble gas mixtures. Because ideal-gas molecules do not interact with each other, the selectivity results are directly applicable to multicomponent systems. To provide insights for materials design, we identify the promising candidates based on the ideal selectivity predicted from the theoretical models discussed above. In addition, the structure−performance relationships are analyzed for both types of nanoporous materials.

Figure 2 shows the adsorption selectivity versus adsorption capacity at the ideal limit for three pairs of noble gas separation. For gas adsorption in a nanoporous material, Henry's constant is determined exclusively by the external potential. The maximum adsorption selectivity (Xe/Ar > Xe/Kr > Kr/Ar) is consistent with the general trend of the difference in LJ parameters, i.e., $\varepsilon_{Xe} > \varepsilon_{Kr} > \varepsilon_{Ar}$ and $\sigma_{Xe} > \sigma_{Kr} > \sigma_{Ar}$ for both MOFs and COFs. Since Xe and Ar have the most different LJ parameters among all three pairs, the separation selectivity of Xe/Ar is the highest, as shown in Figure 2C. In all cases, the maximum adsorption selectivity is much higher than that for the isotopic methane separation because of the larger difference in the LJ parameters.

In contrast to our previous work in the separation of isotopic molecules,[48] the adsorption selectivity increases with the adsorption capacity of the noble gas as measured by Henry's constant for the heavier species in both MOFs and COFs. We calculated Henry's constants for different pairs of noble gases in carbon slit pores in which the interaction of each gas molecule with the surface is represented by the Steele 10-4-3 wall potential.[49] As shown in Figure S1, Henry's constant and adsorption selectivity exhibit strong peaks when the pore width is approximately twice the molecular diameter. Qualitatively,

https://doi.org/10.1021/acsanm.1c03907
ACS Appl. Nano Mater. XXXX, XXX, XXX−XXX

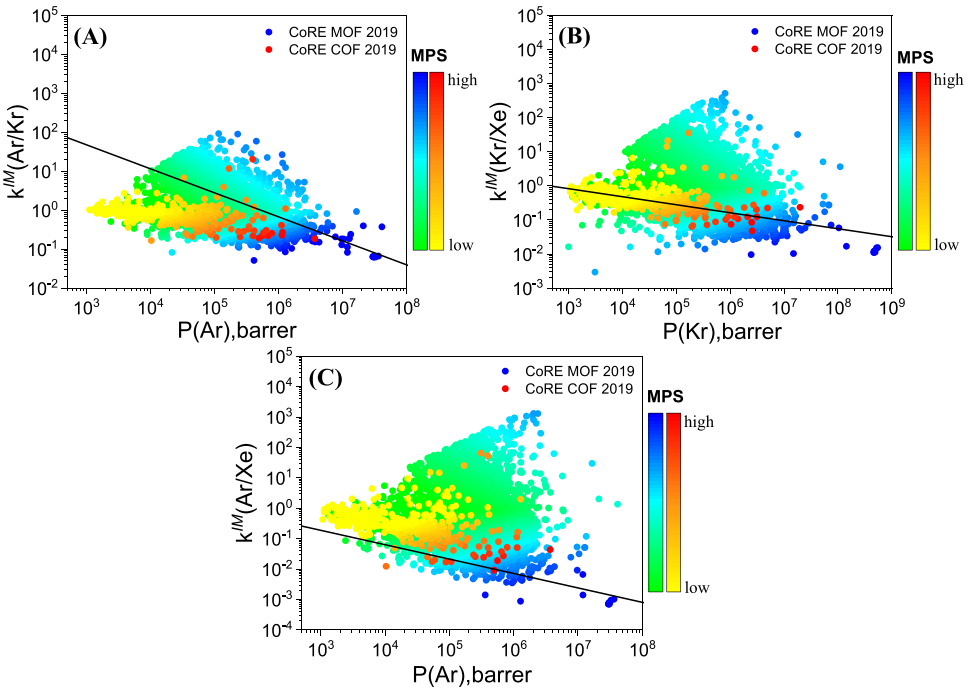

Figure 3. Ideal membrane selectivity versus the permeability for MOFs and COFs from the CoRE 2019 database for the separation of (A) Kr/Ar, (B) Xe/Kr, and (C) Xe/Ar at 300 K. Here, the solid black line represents the Robeson boundary.

the slit-pore model yields the same trends of adsorption selectivity versus Henry's constant (shown in Figure S2) as those shown in Figure 2. Because noble gas molecules have a much larger difference in molecular size than isotopic molecules, when the pore size is more attractive to the smaller noble gas molecule, it is still repulsive to the larger noble gas molecule, which results in the concurrent peak for adsorption selectivity and capacity in the same pore size.

Compared to typical MOFs, COFs have larger inherent pores but smaller specific surface areas (Figure S3A). As a result, COF adsorbents cannot reach the high adsorption capacity and selectivity limit in MOF adsorbents for all three pairs of noble gases shown in Figure 2. Tables S2 and S3 list the top five MOFs and top five COFs, respectively, ranked according to the ideal adsorption selectivity for separating the three noble gas pairs (Kr/Ar, Xe/Kr, and Xe/Ar) at 300 K. Interestingly, the COF adsorbent, COF-367-Co, ranked at the top for all three noble gas pairs. This material was originally reported by Yaghi and co-workers in 2015 as one of 2D Co(II) Por-COFs (2D porphyrin-based COFs).[50,51] It has a specific surface area (1257.96 Å^2/g) and porosity (0.80736) higher than those of most COFs in the database, making it a promising candidate for all kinds of noble gas separations.

3.2. Membrane Separation by MOFs and COFs. While high-throughput screening of nanoporous materials for adsorption separation of noble gas molecules has been widely discussed in the literature,[9,12,24,26] very few studies are concerned with membrane separation despite its superior separation performance by sieving gas with the difference in both sorption and diffusion properties. In this work, with our efficient computational tools, we are able to investigate the potential usage of nanoporous materials as the membrane for the separation of noble gas. For gas separation by a selective membrane, the capacity is defined by the permeability, i.e., the product of Henry's constant and self-diffusion coefficient. The membrane performance score (MPS) is defined by the selectivity multiplied by the permeability:

$$\mathrm{MPS} = S_{\mathrm{fast/slow}} \times P_{\mathrm{fast}} \tag{7}$$

where $S_{\mathrm{fast/slow}}$ stands for the membrane selectivity of the fast-diffusing species over the slow-diffusing species, and P_{fast} is the permeability of the fast-diffusing species. Like the adsorbent performance score, MPS allows us to evaluate the overall performance of membrane separation processes as it considers both separation selectivity and capacity.

Figure 3 shows both MOF and COF membrane selectivity versus the permeability for all three pairs of noble gas molecules. Membranes composed of nanoporous materials (i.e., MOFs and COFs) show excellent membrane selectivity and capacity for noble gas separation. Figure 3 also shows the Robeson boundaries that describe the upper limit of the correlation between selectivity and permeability according to the performance of state-of-art polymer membranes for noble gas separation.[52] Most MOF and COF candidates surpassed the Robeson boundary, which indicates that MOF and COF materials will perform much better than the state-of-art polymer membranes for the separation of noble gas mixtures. Among all three pairs of noble gas molecules, Xe/Ar has the highest number of material candidates that exceed the Robeson boundary because of the large difference in the physicochemical properties (interaction energy and molecular size) between Xe and Ar compared to the other two noble gas pairs.

Tables 2 and 3 list the top five MOFs and top five COFs with the highest membrane selectivity for the separation of three pairs of noble gases. The detailed sorption and diffusion properties for the top five MOFs and top five COFs can be found in Tables S4 and S5. Compared with MOFs, the highest membrane selectivity for COFs is much smaller for all three noble gas pairs, while the permeability values of the two types of nanoporous materials are relatively close to each other. The

https://doi.org/10.1021/acsanm.1c03907
ACS Appl. Nano Mater. XXXX, XXX, XXX−XXX

Table 2. Separation Performance and Metal Sites of the Top Five MOFs Ranked According to Ideal Membrane Selectivity for Each of Three Noble Gas Pairs (Ke/Ar, Xe/Kr, and Xe/Ar) at 300 K[a]

MOF	metal site	k^{IM}(Ar/Kr)	MPS
Kr/Ar			
KOLYUH	Cu	92.67	1.08×10^7
XAJZOY	Al	90.14	2.08×10^7
TAFBEJ	Cd	71.79	6.17×10^6
NETRIN	Zn, Al	64.86	8.69×10^6
HIDBIH	Cd	64.21	8.09×10^6
	metal site	k^{IM}(Kr/Xe)	MPS
Xe/Kr			
LIVREP	Zn	515.6	4.14×10^8
JOVWOI	Fe, Al	387.5	2.73×10^8
GEGGIK01	Co	343.3	2.43×10^8
FUVDEH06	Zn	*337.3*	3.53×10^8
CAHQOS	Al	314.1	1.45×10^8
	metal site	k^{IM}(Ar/Xe)	MPS
Xe/Ar			
MISQIQ07	Al	*1404*	5.89×10^{13}
MISQIQ02	Al	*1403*	6.05×10^{13}
MISQIQ01	Al	*1386*	5.73×10^{13}
LIVREP	Zn	1313	2.68×10^9
JOVWOI	Fe, Al	1306	3.10×10^9

[a]The membrane selectivity in italic font with underline indicates that the original selectivity is less than 1.

Table 3. Separation Performance and Topology of the Top Five COFs Ranked According to Ideal Membrane Selectivity for Each of Three Noble Gas Pairs (Ke/Ar, Xe/Kr, and Xe/Ar) at 300 K[a]

COF	topology	k^{IM}(Ar/Kr)	MPS
Kr/Ar			
PI-COF-2	hcb	20.37	8.06×10^6
Tp-Por-COF-AB	hcb	11.77	1.98×10^6
LZU-301-activated	dia	6.834	2.28×10^5
AEM-COF-2	hcb	*5.980*	3.40×10^5
COF-367-Co	sql	*5.376*	1.07×10^8
	topology	k^{IM}(Kr/Xe)	MPS
Xe/Kr			
N-COF	hcb	35.72	6.07×10^6
COF-DL229_6	dia	21.17	1.47×10^6
DaTp-COF	hcb	*20.91*	1.13×10^9
TPE-COF-II	sql	*15.64*	4.74×10^7
CTF-fuma	hcb	*14.48*	4.26×10^7
	topology	k^{IM}(Ar/Xe)	MPS
Xe/Ar			
DaTp-COF	hcb	*108.1*	5.82×10^9
AEM-COF-2	hcb	*80.16*	6.64×10^7
N-COF	hcb	65.49	2.04×10^7
SIOC-COF-5	bex	*58.37*	2.99×10^8
DPP-TAPP-COF	sql	*56.87*	3.44×10^8

[a]The membrane selectivity in italic font with underline indicates that the original selectivity is less than 1.

larger aperture in COFs leads to a smaller difference in the diffusion coefficient between noble gas molecules in COFs than that in MOFs. As a result, membrane selectivity for top COFs in separating noble gas molecules is much smaller than that for top MOFs. Due to the large aperture of COF materials, the diffusion coefficients of noble gas molecules in most COFs are higher than those in MOFs. However, the solubility (i.e., adsorption capacity) of COFs, as measured by Henry's constant, is typically much lower than that of MOFs due to smaller specific surface areas in COFs. The opposite trends of sorption and transport properties result in similar permeability and MPS values for top MOF and COF candidates with the highest membrane selectivity for noble gas separation. In addition, it is worth noticing that, for promising MOF and COF membrane candidates, a high MPS value favors high permeability because it is easier to improve permeability than the selectivity for the separation of noble gases. As shown in Figure S4, compared with adsorption separation, membrane separation with MOFs and COFs has a much higher selectivity when the difference in interaction energy and molecular size is relatively small such as for Kr/Ar and Xe/Kr, whereas adsorption separation with MOFs and COFs is preferential when the large difference in physicochemical properties exists between noble gas molecules (e.g., Xe/Ar).

3.3. Validation of Theoretical Prediction via Molecular Simulation. Although the accuracy of our theoretical models compared to molecular simulations has been discussed in details in our previous work, we further verified the theoretical prediction of sorption and transport properties with molecular simulations (e.g., GCMC and MD simulation). Since molecular simulations are much more expensive than our theoretical models, only MOFs and COFs with top separation performance are verified with molecular simulations. Figure 4 shows the comparison of Henry's constants and diffusion coefficients between theoretical models and molecular simulations for top MOFs and COFs.

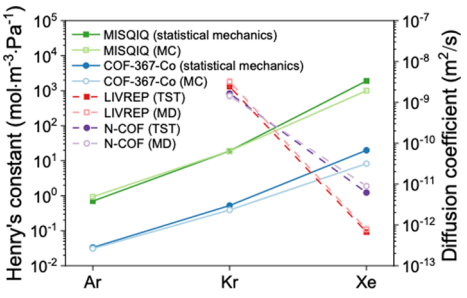

Figure 4. Henry's constants (solid line) for top MOF (MISQIQ) and COF (COF-367-Co) adsorbents were obtained both by the statistical mechanics and by Monte Carlo simulation. The diffusion coefficients (dashed line) for the top MOF (LIVREP) and COF (N-COF) membranes were calculated by transition state theory (TST) and by molecular dynamics simulation.

As shown in Figure 4, Henry's constant calculated from GCMC agrees well with the calculated one according to statistical mechanics. For GCMC simulation, Henry's constant is fitted from the adsorption isotherms of noble gases in the best MOF (MISQIQ) and COF (COF-367-Co) with the highest ideal adsorption selectivity of noble gas (shown in Figure S5). With IAST, one can predict the selectivity of the gas mixture with alike molecules under different operating conditions based on single-component adsorption isotherm.[53] Consistent with Henry's constant, the adsorption amount and selectivity of noble gas in MISQIQ are larger than those in COF-367-Co in the low-pressure region, which also suggests that MISQIQ is a better candidate than COF-367-Co for

https://doi.org/10.1021/acsanm.1c03907
ACS Appl. Nano Mater. XXXX, XXX, XXX−XXX

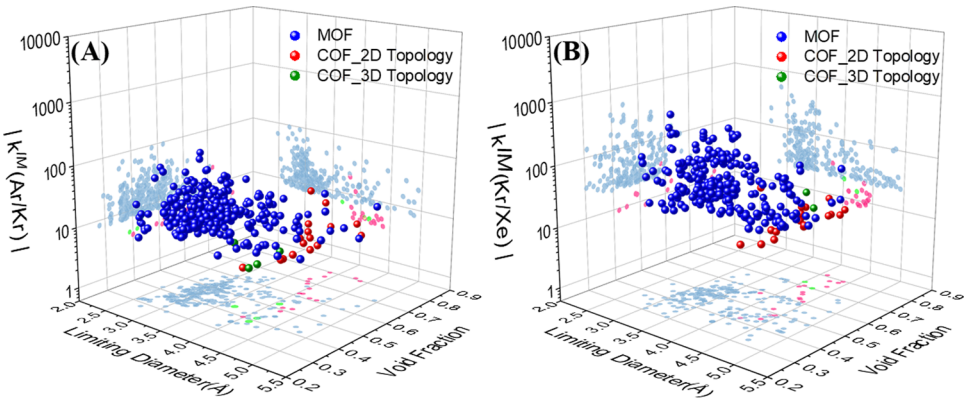

Figure 5. Ideal membrane selectivity versus the pore limiting diameter (PLD) and void fraction of top 5% MOFs and the ideal membrane selectivity versus the diffusion limiting diameter (DLD) and void fraction of top 5% COFs for the separation of (A) Ar/Kr and (B) Kr/Xe binary mixtures at 300 K.

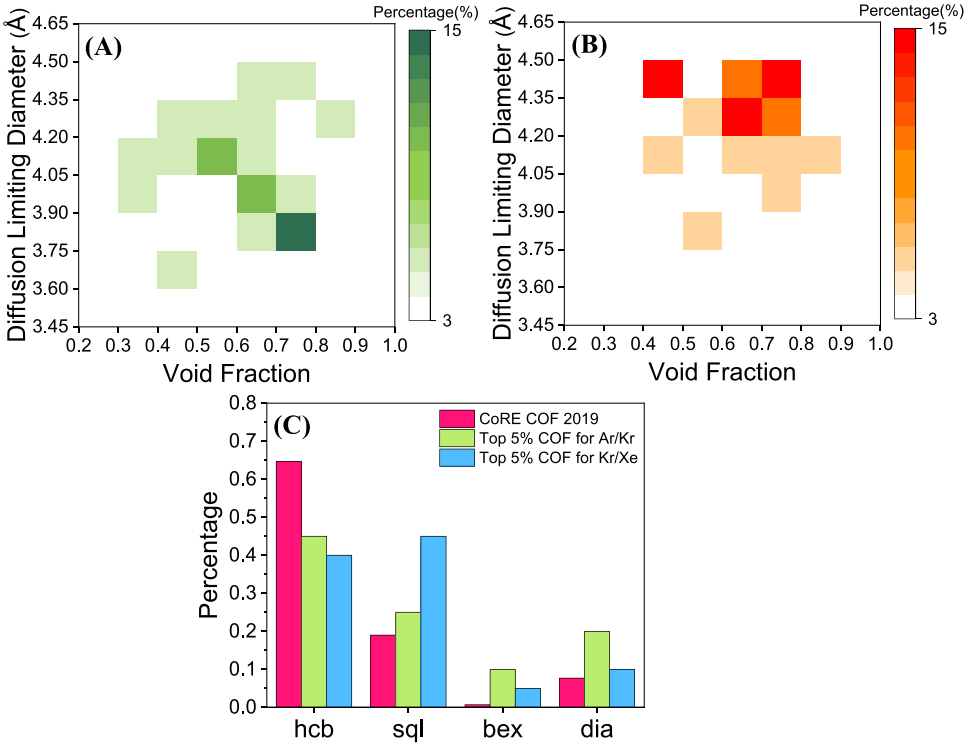

Figure 6. Distributions of the top 5% COFs in terms of the diffusion limiting diameter and the void fraction ranked according to the membrane selectivity for separation of (A) Ar/Kr and (B) Kr/Xe at 300 K. (C) Topology distribution in the COF database and top 5% COFs for the separation of Ar/Kr and Kr/Xe.

adsorption separation of the noble gas. It is also worth noticing that the separation selectivity of noble gas decreases significantly with the increase of pressure for both MISQIQ and COF-367-Co (shown in Figure S5). A similar trend can also be observed in the top five MOFs and COFs with the highest adsorption selectivity of noble gas (shown in Figures S6 and S7). It is because, with the increase of pressure, adsorbate−adsorbate interaction becomes more important than adsorbate−adsorbent interaction and the interaction between noble gas molecules is more similar to that between noble gas molecules and nanoporous materials. As a result, the adsorption selectivity has a sharp drop from ideal adsorption selectivity and approaches 1 when the pressure increases. It is also worth mentioning that the computational cost for GCMC simulation is much more expensive than the theoretical methods. For MISQIQ, the computational time costs 12∼40 CPU hours depending on the system pressure, which would be a huge burden for large-scale screening of nanoporous materials as adsorbents, whereas the theoretical method only takes up to several minutes and even several seconds if GPU-accelerated implementation is used.[54]

Among all three pairs of noble gas molecules considered in this work, the separation of Xe/Kr is the most important one because of its relevance in purifying used nuclear fuel off-gas. Therefore, top MOF (LIVREP) and COF (N-COF) with the highest membrane selectivity are used to benchmark the self-diffusion coefficient calculated from MD simulation and our theoretical approach. As shown in Figure 4, there is an excellent agreement between the self-diffusion coefficient calculated from MD and that from TST at the limit of infinite

https://doi.org/10.1021/acsanm.1c03907
ACS Appl. Nano Mater. XXXX, XXX, XXX−XXX

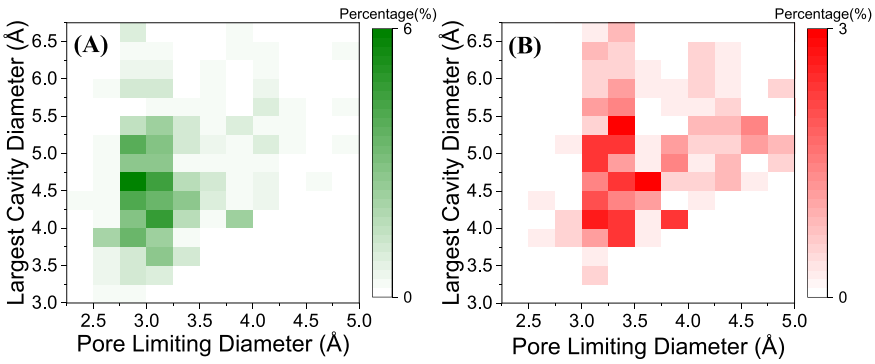

Figure 7. Distributions of the top 5% MOFs in terms of the pore limiting diameter and the largest cavity diameter ranked according to the membrane selectivity for separation of (A) Ar/Kr and (B) Kr/Xe at 300 K.

dilution. While hundreds of CPU hours are needed in MD simulation for fast and intermediate diffusion in nanoporous materials in order to generate long enough displacement, MD simulation becomes computationally prohibitive for slow diffusion (less than 1×10^{-13} m^2/s) in nanoporous materials.[33] However, the computational cost for the simplified string method is independent from the scale of self-diffusion rate, which generally takes less than half a minute with GPU-accelerated implementation.[41] For both sorption and transport properties (viz. Henry's constant and self-diffusion coefficient) of noble gas molecules in nanoporous materials investigated in this work, not only excellent agreements of numerical values exist between theoretical approaches and molecular simulations, but also the significant reduction of computational cost highlights the value of theoretical approaches for large-scale screening of nanoporous materials in gas separation.

3.4. Structure–Performance Relationships. MOF and COF structures are exceptionally diverse. Virtually infinite nanoporous materials can be constructed by the combination of different secondary building blocks. While MOFs consist of metal clusters, organic linkers, and topologies, COFs are composed of organic linkers and topologies. As discussed above, for gas pairs of more practical interest (Ar/Kr and Kr/Xe), membrane separation is more effective than adsorption separation. Therefore, in this section, we analyzed structural features of top MOFs and COFs with the highest membrane selectivity for Ar/Kr and Kr/Xe.

Figure 5 shows the ideal membrane selectivity versus porosity and the limiting diameters for top MOFs and COFs. While the PLD is used for MOFs as the limiting diameter, the diffusion limiting diameter (DLD) is used as the limiting diameter for COFs (shown in Figure S3B). Different from MOFs that have relatively more confined pore structures, COFs have much larger pore structures. In addition, MEP in COFs does not necessarily go through the pore at the center of the pore channel. Therefore, we calculate the shortest distance to the atom in COFs along the MEP as half of the DLD. Benefiting from more confined geometry (i.e., smaller limiting diameter), top MOFs are able to reach a much higher membrane selectivity than top COFs. In Figure 5, one can see that 3D-COFs have generally smaller DLD among the top 5% COF membranes. A similar trend of the inherent pore size can also be observed for the CoRE COF 2019 database (shown in Figure S8A). It is because the 3D network in COFs is self-assembled into the interpenetrated structure, which not only increases the stability of monomeric structures but also leads to the shrinkage of pore channels.[55]

Figure 6A, B presents the DLD versus void fraction for COFs with top 5% membrane selectivity. One can see that the distribution of DLD is concentrated in the range of 3.75∼4.2 Å and 4.2∼4.5 Å for Ar/Kr and Kr/Xe, respectively. Since the molecular size of Kr and Xe is slightly larger than that of Ar and Kr, DLD for COFs with the top 5% membrane selectivity of Kr/Xe is larger than that of Ar/Kr. Different from DLD, the void fraction is relatively evenly distributed between 0.4 and 0.8. The highest membrane selectivity, especially for Xe/Kr, is achieved in COFs with an intermediate void fraction (∼0.6) (shown in Figure S8C), indicating that a neither too dense nor too sparse COF structure would be more likely to have a higher membrane selectivity.[56]

There are eight 2D-topologies [**hcb** (honeycomb), **sql** (square lattice), **hxl** (hexagonal), **fes**, **fxt**, **kgm** (kagome), **bex**, and **kgd** (kagome-dual)] and five 3D-topologies [**ctn** (cubic-C_3N_4), **bor** (boracite), **dia** (diamond), **pts** (platinum sulfide), and **srs** (strontium silicide)] in the CoRE COF 2019 database.[57−60] The majority of promising COF membrane candidates with high membrane selectivity have 2D-**hcb**, 2D-**sql**, or 3D-**dia** topology. In the CoRE COF 2019 database, over 60% COFs have 2D-**hcb** topology, which leads to 2D-**hcb** being a popular topology in top COFs with the highest membrane selectivity as well. It is worth noticing that the percentage of 2D-**sql**, 3D-**dia**, and especially 2D-**bex** topology in top COF candidates is much higher than that in the original database, suggesting that COFs with those topologies are also worthwhile for further experimental and computational design for an even higher membrane selectivity in noble gas separation (shown in Figure 6C). In the original database, COFs with 3D topology are much less than those with 2D topology because the absence of $\pi-\pi$ stacking leads to less-stable 3D structures compared to 2D structures.[61] Despite the challenge to synthesize 3D COFs due to crystallization issues,[62] many top COFs with the highest membrane selectivity are still composed of 3D topology (3D-**dia**), which is not only a relatively stable 3D structure but also the default structure when the tetrahedra are connected.[63−65]

Structural features of promising MOFs for the separation of Ar/Kr and Kr/Xe are also analyzed. Figure 7 shows the distribution of top 5% MOFs with the highest membrane selectivity of Ar/Kr and Kr/Xe in terms of their PLD and LCD. While most top MOFs for membrane separation of Ar/Kr have PLD in the range of 2.75∼3.25 Å and LCD in the range of 3.75∼5.25 Å, most top MOFs for membrane separation of Kr/Xe have the PLD in the range of 3∼4 Å and LCD in the range of 3.75∼5.5 Å. Similar to COFs, due to

https://doi.org/10.1021/acsanm.1c03907
ACS Appl. Nano Mater. XXXX, XXX, XXX−XXX

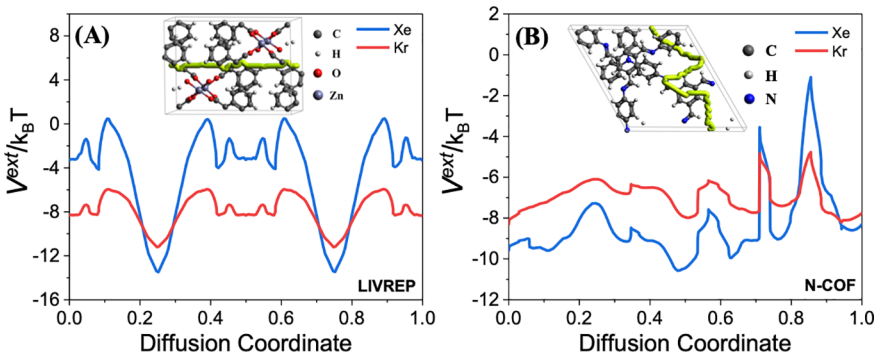

Figure 8. Schematic of the minimum energy path and energy profile of (A) top MOF membrane (LIVREP) and (B) top COF membrane (N-COF) for the separation of Kr/Xe. The yellow line represents the minimum energy pathway of Xe.

the molecular size of noble gas molecules (Xe > Kr > Ar), top MOFs with the highest membrane selectivity sieve Kr/Xe with slightly larger PLD and LCD than Ar/Kr. Although the structure−property relationship for both adsorption and membrane separation is examined near ideal limit, it provides direct insights on the design of nanoporous materials, while the separation performance at finite loading is mostly dominated by gas−gas interactions instead of host−gas interactions.

Among all three pairs of noble gas molecules, the separation of Kr/Xe is of the most practical interest. The MEPs and minimum energy landscapes along the MEPs of Kr and Xe in top MOF (LIVREP) and COF (N-COF) with the highest membrane selectivity of Kr/Xe are shown in Figure 8, and their detailed sorption and transport properties for Xe and Kr are available in Table S8. The membrane selectivity of Kr/Xe of the best MOF, LIVREP, (515.63) is much higher than that of the best COF, N-COF, (35.72) because LIVREF (PLD = 2.88 Å; LCD = 3.92 Å) has a much smaller window diameter along with the MEP than N-COF (DLD = 3.81 Å and DCD = 5.45 Å). In addition, metal atoms (e.g., Zn) in MOFs exert stronger interatomic interaction with the gas molecules, which leads to more repulsion to gas molecules at the transition state and a larger energy barrier difference between Kr and Xe in LIVREP than in N-COF. As a result, LIVREP has a higher diffusion selectivity of Kr/Xe but smaller diffusion coefficients of both Kr and Xe. Although LIVREP has a slightly smaller diffusion coefficient of Xe and Kr than N-COF, the much higher solubility (viz., Henry's constant) helps it maintain a larger permeability at 300 K. According to the screening of the latest CoRE MOF and COF database, MOFs would be a better candidate than COFs for the membrane separation of noble gas, especially Xe/Kr. A higher membrane selectivity can also be expected with careful modification of chemical composition and structure on the best candidate identified in this work.

4. CONCLUSIONS

In this work, we analyzed a large library of computation-ready, experimental nanoporous materials (i.e., MOFs and COFs) for noble gas separation via adsorption separation and membrane separation. The materials database includes 10,143 MOFs and 449 COFs. The sorption and transport properties (viz., Henry's constant and self-diffusion coefficient) are calculated to evaluate their performance as adsorbents or membranes for the separation of commercially valuable noble gases (Ar/Kr, Kr/Xe, and Xe/Ar) in terms of adsorption selectivity and membrane selectivity. Henry's constants and the self-diffusion coefficients predicted by theoretical models agree well with those from molecular simulations with much lower computational cost, which empowers the comprehensive screening of nanoporous materials for membrane separation. When MOFs and COFs are used as an adsorbent, we identify MOF MISQIQ and COF COF-367-Co as the best candidates with the highest adsorption selectivity for all three pairs of noble gas mixtures. As adsorbents, most COFs yield a smaller selectivity than MOFs for all three target gas pairs. For Ar/Kr and Kr/Xe separations, both MOFs and COFs yield a higher selectivity when used as membranes than adsorbents. Because of more confined geometry, the increase of separation selectivity from adsorption separation to membrane separation is more significant for MOFs than for COFs. For the separation of Ar/Xe, separation selectivity in adsorption separation is similar to that in membrane separation.

In general, MOFs have a higher selectivity than COFs when used as membranes for noble gas separation. For Kr/Xe separation, which is the most important noble gas pair for practical application, we identify MOF LIVREP as the best nanoporous material for membrane separation in terms of separation selectivity. It shows an excellent ideal membrane selectivity of 515.63. In comparison with MOFs, the molecular sieving effect in COFs is less significant because of large pore aperture and weaker intermolecular interaction along the minimum energy path. As a result, the diffusion barrier along the MEP in COFs is much lower than that in MOFs, which leads to a smaller membrane selectivity but a higher diffusion coefficient in COFs. In both adsorption and membrane separations, the highest selectivity of MOFs and COFs for three pairs of noble gases follows the same trend of Xe/Ar > Xe/Kr > Kr/Ar because of the decreased difference in the physicochemical properties (i.e., molecular size and interaction energy) between the gas molecules.

For top 5% COFs with the highest membrane selectivity, the void fraction is around 0.6 and the diffusion limiting diameter is mainly distributed in the range of 3.75∼4.2 and 4.2∼4.5 Å for Ar/Kr and Kr/Xe, respectively. Most of these top COF materials have 2D-**hcb**, 2D-**sql**, 2D-**bex** or 3D-**dia** topologies. Similar to the inherent pore size distribution, top COFs with 3D topology in membrane separation have relatively smaller pore sizes than those with 2D topology, which results from the channel shrunk due to interpenetrations and leads to a higher membrane selectivity in COFs with 3D topology than that with 2D topology. On the other hand, the top 5% MOF-membranes for separating Kr/Xe have PLD in the range of 3∼4 Å and LCD in the range of 3.75∼5.5 Å, while top MOFs have PLD in

https://doi.org/10.1021/acsanm.1c03907
ACS Appl. Nano Mater. XXXX, XXX, XXX−XXX

the range of 2.75∼3.25 Å and LCD in the range of 3.75∼5.25 Å for the separation of Ar/Kr.

The structure−performance analysis indicates that the construction of framework materials with the PLD similar to the molecular size is of vital importance for further material design and performance optimization in membrane separation. Based on the understanding of structure−property relationships, the CoRE MOF/COF database provides us with a better perspective on the future exploration of these nanoporous structures. The efficient separation of noble gases will have a broad prospect of applications such as commercial lightning, industrial production, and medical fields.

■ ASSOCIATED CONTENT

Supporting Information

The Supporting Information is available free of charge at https://pubs.acs.org/doi/10.1021/acsanm.1c03907.

Computational details of theoretical frameworks and molecular simulation for the separation of noble gases in nanoporous materials, including the adsorption isotherms, diffusion coefficient verification, separation selectivity for Ar/Kr, Kr/Xe, and Xe/Ar, and the additional comparison of structure−performance relationships between MOFs and COFs at 300 K (PDF)

■ AUTHOR INFORMATION

Corresponding Authors

Diannan Lu − *Department of Chemical Engineering, Tsinghua University, Beijing 100084, China;* orcid.org/0000-0001-5993-5626; Email: ludiannan@mail.tsinghua.edu.cn

Jianzhong Wu − *Department of Chemical and Environmental Engineering, University of California, Riverside, California 92521, United States;* orcid.org/0000-0002-4582-5941; Email: jwu@engr.ucr.edu

Authors

Jingqi Wang − *Department of Chemical Engineering, Tsinghua University, Beijing 100084, China;* orcid.org/0000-0001-6805-4222

Musen Zhou − *Department of Chemical and Environmental Engineering, University of California, Riverside, California 92521, United States;* orcid.org/0000-0002-2848-8939

Weiyang Fei − *Department of Chemical Engineering, Tsinghua University, Beijing 100084, China*

Complete contact information is available at: https://pubs.acs.org/10.1021/acsanm.1c03907

Notes

The authors declare no competing financial interest.

■ ACKNOWLEDGMENTS

The authors would like to express appreciation for the support of the National Natural Science foundation of China, No. U1862204 and 21878175, and the State Key Laboratory of Chemical Engineering with Grant No. SKL-CHE-20.

■ REFERENCES

(1) Halka, M.; Nordstrom, B., *Halogens and Noble Gases*; Infobase publishing: 2010.

(2) Asimov, I., *The noble gases*; Basic Books: 1966.

(3) Marshall, J.; Bird, A. C. A comparative histopathological study of argon and krypton laser irradiations of the human retina. *Br. J. Ophthalmol.* **1979**, *63*, 657−668.

(4) Wang, Q.; Ke, T.; Yang, L.; Zhang, Z.; Cui, X.; Bao, Z.; Ren, Q.; Yang, Q.; Xing, H. Separation of Xe from Kr with Record Selectivity and Productivity in Anion-Pillared Ultramicroporous Materials by Inverse Size-Sieving. *Angew. Chem. Int. Ed. Engl.* **2020**, *59*, 3423−3428.

(5) Cox, P., *The Kirk-Othmer encyclopedia of chemical technology: Volume 2, Alkanolamines to Antibiotics (Glycopeptides)*. Kroschwitz, J. I.; Howe-Grant, M.; Humphreys, L. C.; Gray, L. (editors); Wiley-Interscience: Chichester, 1992 xxviii+ 1018.£ 135.00. Elsevier: 1993.

(6) Kerry, F. G., *Industrial gas handbook: gas separation and purification*; CRC press: 2007.

(7) Guo, F.; Liu, Y.; Hu, J.; Liu, H.; Hu, Y. Fast screening of porous materials for noble gas adsorption and separation: a classical density functional approach. *Phys. Chem. Chem. Phys.* **2018**, *20*, 28193−28204.

(8) Ryan, P.; Farha, O. K.; Broadbelt, L. J.; Snurr, R. Q. Computational screening of metal-organic frameworks for xenon/krypton separation. *AIChE J.* **2011**, *57*, 1759−1766.

(9) Sumer, Z.; Keskin, S. Molecular simulations of MOF adsorbents and membranes for noble gas separations. *Chem. Eng. Sci.* **2017**, *164*, 108−121.

(10) Chen, C.; Feng, X.; Zhu, Q.; Dong, R.; Yang, R.; Cheng, Y.; He, C. Microwave-Assisted Rapid Synthesis of Well-Shaped MOF-74 (Ni) for CO2 Efficient Capture. *Inorg. Chem.* **2019**, *58*, 2717−2728.

(11) Wang, B.; Xie, L.-H.; Wang, X.; Liu, X.-M.; Li, J.; Li, J.-R. Applications of metal−organic frameworks for green energy and environment: New advances in adsorptive gas separation, storage and removal. *Green Energy Environ.* **2018**, *3*, 191−228.

(12) Tong, M.; Lan, Y.; Yang, Q.; Zhong, C. Exploring the structure-property relationships of covalent organic frameworks for noble gas separations. *Chem. Eng. Sci.* **2017**, *168*, 456−464.

(13) Côté, A. P.; Benin, A. I.; Ockwig, N. W.; O'Keeffe, M.; Matzger, A. J.; Yaghi, O. M. Porous, crystalline, covalent organic frameworks. *Science* **2005**, *310*, 1166−1170.

(14) Oh, H.; Savchenko, I.; Mavrandonakis, A.; Heine, T.; Hirscher, M. Highly effective hydrogen isotope separation in nanoporous metal-organic frameworks with open metal sites: direct measurement and theoretical analysis. *ACS Nano* **2014**, *8*, 761−770.

(15) Zhou, M.; Tian, Y.; Fei, W.; Wu, J. Fractionation of Isotopic Methanes with Metal−Organic Frameworks. *J. Phys. Chem. C* **2019**, *123*, 7397−7407.

(16) Gurdal, Y.; Keskin, S. Atomically Detailed Modeling of Metal Organic Frameworks for Adsorption, Diffusion, and Separation of Noble Gas Mixtures. *Ind. Eng. Chem. Res.* **2012**, *51*, 7373−7382.

(17) Kancharlapalli, S.; Natarajan, S.; Ghanty, T. K. Confinement-Directed Adsorption of Noble Gases (Xe/Kr) in MFM-300(M)-Based Metal−Organic Framework Materials. *J. Phys. Chem. C* **2019**, *123*, 27531−27541.

(18) Soleimani Dorcheh, A.; Denysenko, D.; Volkmer, D.; Donner, W.; Hirscher, M. Noble gases and microporous frameworks; from interaction to application. *Microporous Mesoporous Mater.* **2012**, *162*, 64−68.

(19) Kim, H.; Yang, S.; Rao, S. R.; Narayanan, S.; Kapustin, E. A.; Furukawa, H.; Umans, A. S.; Yaghi, O. M.; Wang, E. N. Water harvesting from air with metal-organic frameworks powered by natural sunlight. *Science* **2017**, *356*, 430−434.

(20) Liu, J.; Strachan, D. M.; Thallapally, P. K. Enhanced noble gas adsorption in Ag@MOF-74Ni. *Chem. Commun.* **2014**, *50*, 466−468.

(21) Perry, J. J., IV; Teich-McGoldrick, S. L.; Meek, S. T.; Greathouse, J. A.; Haranczyk, M.; Allendorf, M. D. Noble Gas Adsorption in Metal−Organic Frameworks Containing Open Metal Sites. *J. Phys. Chem. C* **2014**, *118*, 11685−11698.

(22) Fan, H.; Mundstock, A.; Feldhoff, A.; Knebel, A.; Gu, J.; Meng, H.; Caro, J. Covalent Organic Framework-Covalent Organic Framework Bilayer Membranes for Highly Selective Gas Separation. *J. Am. Chem. Soc.* **2018**, *140*, 10094−10098.

(23) Xiang, S.; He, Y.; Zhang, Z.; Wu, H.; Zhou, W.; Krishna, R.; Chen, B. Microporous metal-organic framework with potential for carbon dioxide capture at ambient conditions. *Nat. Commun.* **2012**, *3*, 954.
(24) Banerjee, D.; Simon, C. M.; Plonka, A. M.; Motkuri, R. K.; Liu, J.; Chen, X.; Smit, B.; Parise, J. B.; Haranczyk, M.; Thallapally, P. K. Metal-organic framework with optimally selective xenon adsorption and separation. *Nat. Commun.* **2016**, *7*, No. ncomms11831.
(25) Lin, W. Q.; Xiong, X. L.; Liang, H.; Chen, G. H. Multiscale Computational Screening of Metal-Organic Frameworks for Kr/Xe Adsorption Separation: A Structure-Property Relationship-Based Screening Strategy. *ACS Appl. Mater. Interfaces* **2021**, *13*, 17998−18009.
(26) Gurdal, Y.; Keskin, S. Predicting Noble Gas Separation Performance of Metal Organic Frameworks Using Theoretical Correlations. *J. Phys. Chem. C* **2013**, *117*, 5229−5241.
(27) Van Heest, T.; Teich-McGoldrick, S. L.; Greathouse, J. A.; Allendorf, M. D.; Sholl, D. S. Identification of Metal−Organic Framework Materials for Adsorption Separation of Rare Gases: Applicability of Ideal Adsorbed Solution Theory (IAST) and Effects of Inaccessible Framework Regions. *J. Phys. Chem. C* **2012**, *116*, 13183−13195.
(28) Chung, Y. G.; Haldoupis, E.; Bucior, B. J.; Haranczyk, M.; Lee, S.; Zhang, H.; Vogiatzis, K. D.; Milisavljevic, M.; Ling, S.; Camp, J. S.; Slater, B.; Siepmann, J. I.; Sholl, D. S.; Snurr, R. Q. Advances, Updates, and Analytics for the Computation-Ready, Experimental Metal−Organic Framework Database: CoRE MOF 2019. *J. Chem. Eng. Data* **2019**, *64*, 5985−5998.
(29) Chung, Y. G.; Camp, J.; Haranczyk, M.; Sikora, B. J.; Bury, W.; Krungleviciute, V.; Yildirim, T.; Farha, O. K.; Sholl, D. S.; Snurr, R. Q. Computation-Ready, Experimental Metal−Organic Frameworks: A Tool To Enable High-Throughput Screening of Nanoporous Crystals. *Chem. Mater.* **2014**, *26*, 6185−6192.
(30) Yan, T.; Lan, Y.; Tong, M.; Zhong, C. Screening and Design of Covalent Organic Framework Membranes for CO2/CH4 Separation. *ACS Sustainable Chem. Eng.* **2018**, *7*, 1220−1227.
(31) Tong, M.; Yang, Q.; Zhong, C. Computational screening of covalent organic frameworks for CH4/H2, CO2/H2 and CO2/CH4 separations. *Microporous Mesoporous Mater.* **2015**, *210*, 142−148.
(32) Li, L.; Zhang, T.; Duan, Y.; Wei, Y.; Dong, C.; Ding, L.; Qiao, Z.; Wang, H. Selective gas diffusion in two-dimensional MXene lamellar membranes: insights from molecular dynamics simulations. *J. Mater. Chem. A* **2018**, *6*, 11734−11742.
(33) Verploegh, R. J.; Nair, S.; Sholl, D. S. Temperature and Loading-Dependent Diffusion of Light Hydrocarbons in ZIF-8 as Predicted Through Fully Flexible Molecular Simulations. *J. Am. Chem. Soc.* **2015**, *137*, 15760−15771.
(34) Boato, G.; Casanova, G. A self-consistent set of molecular parameters for neon, argon, krypton and xenon. *Physica* **1961**, *27*, 571−589.
(35) Rappe, A. K.; Casewit, C. J.; Colwell, K. S.; Goddard, W. A., III; Skiff, W. M. UFF, a full periodic table force field for molecular mechanics and molecular dynamics simulations. *J. Am. Chem. Soc.* **1992**, *114*, 10024−10035.
(36) Myers, A. L.; Prausnitz, J. M. Thermodynamics of mixed-gas adsorption. *AIChE J.* **1965**, *11*, 121−127.
(37) Haldoupis, E.; Nair, S.; Sholl, D. S. Efficient calculation of diffusion limitations in metal organic framework materials: a tool for identifying materials for kinetic separations. *J. Am. Chem. Soc.* **2010**, *132*, 7528−7539.
(38) Keskin, S.; Sholl, D. S. Efficient Methods for Screening of Metal Organic Framework Membranes for Gas Separations Using Atomically Detailed Models. *Langmuir* **2009**, *25*, 11786−11795.
(39) Tian, Y.; Xu, X.; Wu, J. Thermodynamic Route to Efficient Prediction of Gas Diffusivity in Nanoporous Materials. *Langmuir* **2017**, *33*, 11797−11803.
(40) Frenkel, D.; Smit, B., *Understanding molecular simulation* 2nd edition; Academic Press: London, UK, 2002.
(41) Zhou, M.; Wu, J. Massively Parallel GPU-Accelerated String Method for Fast and Accurate Prediction of Molecular Diffusivity in Nanoporous Materials. *ACS Appl. Nano Mater.* **2021**, *4*, 5394−5403.
(42) Liu, Y.; Fu, J.; Wu, J. Excess-entropy scaling for gas diffusivity in nanoporous materials. *Langmuir* **2013**, *29*, 12997−13002.
(43) Dubbeldam, D.; Beerdsen, E.; Vlugt, T. J. H.; Smit, B. Molecular simulation of loading-dependent diffusion in nanoporous materials using extended dynamically corrected transition state theory. *J. Chem. Phys.* **2005**, *122*, 224712.
(44) Willems, T. F.; Rycroft, C. H.; Kazi, M.; Meza, J. C.; Haranczyk, M. Algorithms and tools for high-throughput geometry-based analysis of crystalline porous materials. *Microporous Mesoporous Mater.* **2012**, *149*, 134−141.
(45) Dubbeldam, D.; Calero, S.; Ellis, D. E.; Snurr, R. Q. RASPA: molecular simulation software for adsorption and diffusion in flexible nanoporous materials. *Mol. Simul.* **2016**, *42*, 81−101.
(46) Hammersley, J., *Monte carlo methods*; Springer Science & Business Media: 2013.
(47) Plimpton, S. Fast Parallel Algorithms for Short-Range Molecular Dynamics. *J. Comput. Phys.* **1995**, *117*, 1−19.
(48) Wang, J.; Zhou, M.; Lu, D.; Fei, W.; Wu, J. Computational screening and design of nanoporous membranes for efficient carbon isotope separation. *Green Energy Environ.* **2020**, *5*, 364−373.
(49) Tian, Y.; Fei, W. Y.; Wu, J. Z. Separation of Carbon Isotopes in Methane with Nanoporous Materials. *Ind. Eng. Chem. Res.* **2018**, *57*, 5151−5160.
(50) Lin, S.; Diercks, C. S.; Zhang, Y. B.; Kornienko, N.; Nichols, E. M.; Zhao, Y.; Paris, A. R.; Kim, D.; Yang, P.; Yaghi, O. M.; Chang, C. J. Covalent organic frameworks comprising cobalt porphyrins for catalytic CO(2) reduction in water. *Science* **2015**, *349*, 1208−1213.
(51) Wang, H.; Ding, H.; Meng, X.; Wang, C. Two-dimensional porphyrin- and phthalocyanine-based covalent organic frameworks. *Chin. Chem. Lett.* **2016**, *27*, 1376−1382.
(52) Robeson, L. M. The upper bound revisited. *J. Membr. Sci.* **2008**, *320*, 390−400.
(53) Fei, S.; Hsu, W. L.; Delaunay, J. J.; Daiguji, H. Molecular dynamics study of water confined in MIL-101 metal-organic frameworks. *J. Chem. Phys.* **2021**, *154*, 144503.
(54) Zhou, M.; Wu, J. A GPU implementation of classical density functional theory for rapid prediction of gas adsorption in nanoporous materials. *J. Chem. Phys.* **2020**, *153*, No. 074101.
(55) Zhu, R.; Ding, J.; Jin, L.; Pang, H. Interpenetrated structures appeared in supramolecular cages, MOFs, COFs. *Coord. Chem. Rev.* **2019**, *389*, 119−140.
(56) Kim, W. K.; Kanduč, M.; Roa, R.; Dzubiella, J. Tuning the Permeability of Dense Membranes by Shaping Nanoscale Potentials. *Phys. Rev. Lett.* **2019**, *122*, No. 108001.
(57) Lyle, S. J.; Waller, P. J.; Yaghi, O. M. Covalent Organic Frameworks: Organic Chemistry Extended into Two and Three Dimensions. *Trends Chem.* **2019**, *1*, 172−184.
(58) Mitina, T. G.; Blatov, V. A. Topology of 2-Periodic Coordination Networks: Toward Expert Systems in Crystal Design. *Cryst. Growth Des.* **2013**, *13*, 1655−1664.
(59) Springer, M. A.; Liu, T. J.; Kuc, A.; Heine, T. Topological two-dimensional polymers. *Chem. Soc. Rev.* **2020**, *49*, 2007−2019.
(60) Guan, X.; Chen, F.; Fang, Q.; Qiu, S. Design and applications of three dimensional covalent organic frameworks. *Chem. Soc. Rev.* **2020**, *49*, 1357−1384.
(61) Kandambeth, S.; Dey, K.; Banerjee, R. Covalent Organic Frameworks: Chemistry beyond the Structure. *J. Am. Chem. Soc.* **2019**, *141*, 1807−1822.
(62) Waller, P. J.; Gándara, F.; Yaghi, O. M. Chemistry of Covalent Organic Frameworks. *Acc. Chem. Res.* **2015**, *48*, 3053−3063.
(63) Uribe-Romo, F. J.; Hunt, J. R.; Furukawa, H.; Klöck, C.; O'Keeffe, M.; Yaghi, O. M. A Crystalline Imine-Linked 3-D Porous Covalent Organic Framework. *J. Am. Chem. Soc.* **2009**, *131*, 4570−4571.

https://doi.org/10.1021/acsanm.1c03907
ACS Appl. Nano Mater. XXXX, XXX, XXX−XXX

(64) Lin, G.; Ding, H.; Yuan, D.; Wang, B.; Wang, C. A Pyrene-Based, Fluorescent Three-Dimensional Covalent Organic Framework. *J. Am. Chem. Soc.* **2016**, *138*, 3302−3305.
(65) Bonneau, C.; Delgado-Friedrichs, O.; O'Keeffe, M.; Yaghi, O. M. Three-periodic nets and tilings: minimal nets. *Acta Crystallogr. Sect. A Found. Crystallogr.* **2004**, *60*, 517−520.

https://doi.org/10.1021/acsanm.1c03907
ACS Appl. Nano Mater. XXXX, XXX, XXX−XXX